Neutron-induced fission cross section of ^{234}U and ^{237}Np measured at the CERN Neutron Time-of-Flight (n_TOF) facility

C. Paradela,[1,*] L. Tassan-Got,[2] L. Audouin,[2,3] B. Berthier,[2] I. Duran,[1] L. Ferrant,[2] S. Isaev,[2] C. Le Naour,[2] C. Stephan,[2] D. Tarrío,[1] D. Trubert,[2] U. Abbondanno,[4] G. Aerts,[5] H. Álvarez,[1] F. Álvarez-Velarde,[6] S. Andriamonje,[7] J. Andrzejewski,[8] P. Assimakopoulos,[9] G. Badurek,[10] P. Baumann,[11] F. Bečvář,[12] E. Berthoumieux,[7] F. Calviño,[13] M. Calviani,[14,15] D. Cano-Ott,[6] R. Capote,[16,17] C. Carrapiço,[7,18] P. Cennini,[19] V. Chepel,[20] E. Chiaveri,[19] N. Colonna,[21] G. Cortes,[22] A. Couture,[23] J. Cox,[23] M. Dahlfors,[19] S. David,[2] I. Dillmann,[3] C. Domingo-Pardo,[24,25] W. Dridi,[7] C. Eleftheriadis,[26] M. Embid-Segura,[6] A. Ferrari,[19] R. Ferreira-Marques,[20] K. Fujii,[4] W. Furman,[27] I. Goncalves,[20] E. González-Romero,[6] F. Gramegna,[14] C. Guerrero,[6] F. Gunsing,[7] B. Haas,[28] R. Haight,[29] M. Heil,[3] A. Herrera-Martinez,[19] M. Igashira,[30] E. Jericha,[10] Y. Kadi,[19] F. Käppeler,[3] D. Karadimos,[9] D. Karamanis,[9] M. Kerveno,[11] P. Koehler,[31] E. Kossionides,[32] M. Krtička,[12] C. Lampoudis,[7,26] H. Leeb,[10] A. Lindote,[20] I. Lopes,[20] M. Lozano,[17] S. Lukic,[11] J. Marganiec,[8] S. Marrone,[21] T. Martínez,[6] C. Massimi,[33] P. Mastinu,[14] A. Mengoni,[16,19] P. M. Milazzo,[4] C. Moreau,[4] M. Mosconi,[3] F. Neves,[20] H. Oberhummer,[10] S. O'Brien,[23] M. Oshima,[34] J. Pancin,[7] C. Papachristodoulou,[9] C. Papadopoulos,[35] N. Patronis,[9] A. Pavlik,[36] P. Pavlopoulos,[37] L. Perrot,[7] M. T. Pigni,[10] R. Plag,[3] A. Plompen,[38] A. Plukis,[7] A. Poch,[22] J. Praena,[14] C. Pretel,[22] J. Quesada,[17] T. Rauscher,[39] R. Reifarth,[29] C. Rubbia,[40] G. Rudolf,[11] P. Rullhusen,[38] J. Salgado,[18] C. Santos,[18] L. Sarchiapone,[19] I. Savvidis,[26] G. Tagliente,[21] J. L. Tain,[24] L. Tavora,[18] R. Terlizzi,[21] G. Vannini,[33] P. Vaz,[18] A. Ventura,[41] D. Villamarin,[6] M. C. Vincente,[6] V. Vlachoudis,[19] R. Vlastou,[35] F. Voss,[3] S. Walter,[3] M. Wiescher,[23] and K. Wisshak[3]

(n_TOF Collaboration)

[1]*Universidade de Santiago de Compostela, Spain*
[2]*Centre National de la Recherche Scientifique/IN2P3-IPN, Orsay, France*
[3]*Forschungszentrum Karlsruhe GmbH (FZK), Institut fürKernphysik, Germany*
[4]*Istituto Nazionale di Fisica Nucleare, Trieste, Italy*
[5]*CEA/Saclay-IRFU, Gif-sur-Yvette, France*
[6]*Centro de Investigaciones Energeticas Medioambientales y Tecnologicas, Madrid, Spain*
[7]*CEA/Saclay-DSM/DAPNIA, Gif-sur-Yvette, France*
[8]*University of Lodz, Lodz, Poland*
[9]*University of Ioannina, Greece*
[10]*Atominstitut der Österreichischen Universitäten, Technische Universität Wien, Austria*
[11]*Centre National de la Recherche Scientifique/IN2P3-IReS, Strasbourg, France*
[12]*Charles University, Prague, Czech Republic*
[13]*Universidad Politecnica de Catalunya, Barcelona, Spain*
[14]*Istituto Nazionale di Fisica Nucleare, Laboratori Nazionali di Legnaro, Italy*
[15]*Dipartimento di Fisica, Università di Padova, Italy*
[16]*International Atomic Energy Agency, Nuclear Data Section, Vienna, Austria*
[17]*Universidad de Sevilla, Spain*
[18]*Instituto Tecnológico e Nuclear, Lisbon, Portugal*
[19]*CERN, Geneva, Switzerland*
[20]*LIP - Coimbra & Departamento de Fisica da Universidade de Coimbra, Portugal*
[21]*Istituto Nazionale di Fisica Nucleare, Bari, Italy*
[22]*Universitat Politecnica de Catalunya, Barcelona, Spain*
[23]*University of Notre Dame, Notre Dame, Indiana, USA*
[24]*Instituto de Física Corpuscular, CSIC-Universidad de Valencia, Spain*
[25]*GSI, Darmstadt, Germany*
[26]*Aristotle University of Thessaloniki, Greece*
[27]*Joint Institute for Nuclear Research, Frank Laboratory of Neutron Physics, Dubna, Russia*
[28]*Centre National de la Recherche Scientifique/IN2P3-CENBG, Bordeaux, France*
[29]*Los Alamos National Laboratory, New Mexico, USA*
[30]*Tokyo Institute of Technology, Tokyo, Japan*
[31]*Oak Ridge National Laboratory, Physics Division, Oak Ridge, Tennessee, USA*
[32]*NCSR, Athens, Greece*
[33]*Dipartimento di Fisica, Università di Bologna, and Sezione INFN di Bologna, Italy*
[34]*Japan Atomic Energy Research Institute, Tokai-mura, Japan*
[35]*National Technical University of Athens, Greece*
[36]*Fakültat für Physik, Universität Wien, Austria*
[37]*Pôle Universitaire Léonard de Vinci, Paris La Défense, France*
[38]*CEC-JRC-IRMM, Geel, Belgium*
[39]*Department of Physics-University of Basel, Switzerland*

[40]*Università degli Studi Pavia, Pavia, Italy*
[41]*ENEA, Bologna, Italy*

A high-resolution measurement of the neutron-induced fission cross section of ^{234}U and ^{237}Np has been performed at the CERN Neutron Time-of-Flight facility. The cross sections have been determined in a wide energy range from 1 eV to 1 GeV using the evaluated ^{235}U cross section as reference. In these measurements the energy determination for the ^{234}U resonances could be improved, whereas previous discrepancies for the ^{237}Np resonances were confirmed. New cross-section data are provided for high neutron energies that go beyond the limits of prior evaluations, obtaining important differences in the case of ^{237}Np.

I. INTRODUCTION

Nuclear reaction data for minor actinides play a key role in the development of a new generation of nuclear reactors. The aim for future reactors is to significantly reduce nuclear-waste radiotoxicity through partitioning and transmutation techniques, thereby decreasing the repository needs for high-level radioactive waste.

Recently, there has been a demand for extensive neutron-induced nuclear cross-section measurements to fulfill the data requirements for these new reactors. Among the minor actinides, ^{234}U and ^{237}Np are included in the priority list suggested by the International Nuclear Data Committee [1,2].

The incineration of ^{237}Np, one of the more abundant isotopes in the spent fuel from current reactors, is an important issue in transmutation. Although ^{234}U plays a limited role in the ^{235}U cycle, it is important for the development of the thorium cycle, where it acts as an analog to ^{240}Pu in the Pu/U cycle of the present-day fast reactors. Most previous measurements of these elements were performed a few decades ago in limited neutron-energy ranges.

The work presented here forms part of the extensive program of fission cross-section measurements that are in progress at the CERN Neutron Time-of-Flight (n_TOF) facility. The aim is to improve the accuracy of nuclear data involved in the transmutation of nuclear waste [3] and the thorium fuel cycle [4].

II. EXPERIMENTAL METHOD

The experiment was performed in two sequential data-taking periods of two weeks each, in which samples of ^{235}U and ^{238}U were used as references. Fission events were detected using a reaction chamber based on parallel-plate avalanche counters (PPACs) developed at IPN-Orsay [5,6].

At the n_TOF facility, a high neutron flux is produced by bombardment of a lead spallation target with 6-ns-wide, intense proton bunches from the Proton Synchrotron complex at CERN. The cooling water surrounding the lead target acts as a moderator to produce the extended energy range of the neutron flux. The long flight path (185 m) to the experimental area provides the possibility for high-resolution time-of-flight (TOF) measurements. n_TOF has made it possible to perform the only fission experiment to date covering the energy range from 1 eV to 1 GeV simultaneously. More detailed characteristics of the facility are described elsewhere [7–9].

A. Parallel plate avalanche counters

The PPACs used in this work are described extensively in Refs. [10,11]. They consist of one central anode surrounded by two cathodes with a low-pressure gas filling the 3-mm gaps between the electrodes. PPAC signals are very fast (10 ns of full width at tenth maximum for the anode signals), which reduces the pileup probabilities. The reaction chamber is composed of ten PPACs and nine targets, one between each pair of detectors, all placed perpendicular to the neutron beam. The two fission products emitted in a fission reaction are detected in coincidence by the PPACs surrounding the fissioning sample (Fig. 1).

The PPACs also supply the fragment position in the detector by means of the information obtained from stripped cathodes. Each cathode consists of 2-mm-wide strips connected to a delay line, which is read by adapted preamplifiers. The time difference between delay line outputs provides a one-dimensional position. By combining the signals from the two orthogonal cathode strips, the position of the crossing particle, and therefore the fission fragment trajectory, can be reconstructed. Nevertheless, during this experiment, there were problems recording the cathode signals and the localization measurement could not be used to determine systematically the detector acceptance, because it introduced an unknown energy dependence of the detection efficiency. Therefore, the cross-section measurements rely only on the anode signals, which are not affected by this drawback.

B. Targets

The actinide samples were between 200 and 300 μg/cm^2 in thickness, electrodeposited on a very thin aluminum foil of 2.5 μm so that both fission fragments could be detected in coincidence. The actinide deposits were 8 cm in diameter, with total masses of about 15 mg. The total masses and their distributions were measured by α counting and Rutherford backscattering spectroscopy (RBS). The RBS method also provides the chemical composition of samples and backings (see Table I) [11].
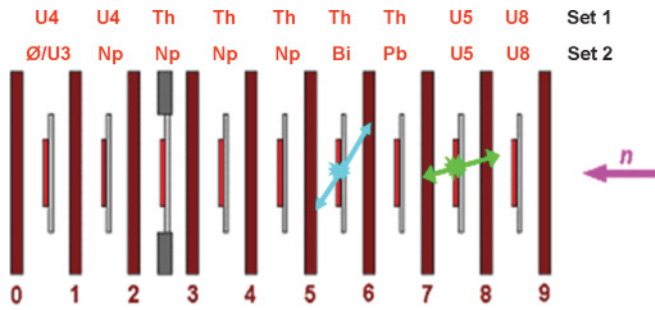
*carlos.paradela@usc.es

FIG. 1. (Color online) Schematic view of the PPAC detection setup used at the n_TOF facility. The samples measured during 2003 are indicated on top.

Two sets of nine samples each were used in the experiment as shown in Fig. 1. The first set included two ^{234}U, five ^{232}Th, one ^{235}U, and one ^{238}U target. The last two samples were used as references to measure the neutron flux and they were common to both target sets. The second set was composed of four ^{237}Np, one ^{233}U, one ^{209}Bi, and one natural lead target along with the two reference targets. The PPACs and the targets are thin enough that even with ten detectors in beam, the neutron flux attenuation is less than 1% in the largest resonances, as confirmed by MCNP calculations [12].

Isotopic impurities were largest in the ^{235}U sample, which contained ^{238}U, ^{234}U, and ^{236}U in atomic proportion to ^{235}U of 6.28%, 0.74%, and 0.27%, respectively. The counting rate of this target has been corrected by a factor which takes into account the fission cross sections of these impurities.

The purity of the ^{237}Np and ^{234}U samples was very high: 99.99% and 99.08%, respectively. The ^{241}Am traces reported in the ^{237}Np samples are not relevant in the counting rate. It is worth mentioning that the composition of the first neptunium target is different from the others, having an americium content five times larger. However, for the ^{234}U targets, the presence of 0.077% of ^{235}U had to be taken into account owing to the high cross section of this fissile isotope at low energies. Its contribution has been verified through resonance identification and removed by subtracting the ^{235}U target counting rate multiplied by the corresponding factor.

C. n_TOF acquisition system

Each PPAC had five preamplifiers (one for the anode and two for each cathode) connected to the Acqiris flash

TABLE I. Sample masses with statistical and systematic uncertainties.

Sample	Mass (mg) ± Stat. ± Syst.
^{235}U	$13.97 \pm 0.02 \pm 0.10$
^{238}U	$11.50 \pm 0.05 \pm 0.08$
^{234}U(1)	$13.39 \pm 0.02 \pm 0.09$
^{234}U(2)	$13.59 \pm 0.02 \pm 0.09$
^{237}Np(1)	$14.25 \pm 0.02 \pm 0.10$
^{237}Np(2)	$16.05 \pm 0.02 \pm 0.11$
^{237}Np(3)	$15.43 \pm 0.02 \pm 0.11$
^{237}Np(4)	$16.13 \pm 0.02 \pm 0.11$

analog-to-digital converters (FADCs) of the n_TOF data-acquisition system [13]. The FADCs were set to collect data during 16 ms after the trigger obtained from a proton beam monitor, corresponding to a minimum neutron energy of 0.7 eV. A zero-suppression algorithm is used to remove unnecessary information from the registered FADC sequences before the remaining data are stored. The low repetition rate of 0.4 Hz allows to transfer the collected data between beam pulses. It also avoids uncorrelated background from wraparound neutrons.

III. DATA ANALYSIS

The fact that the full analog shape of the PPAC signals is digitized has the advantage that dead-time losses are minimized, but results in a huge amount of data. Therefore, a preliminary treatment takes place in the translation of raw data to data summary tape (DST), n_TOF format for off-line analyses.

A. Raw-data treatment

We have implemented a digital filter to discriminate true signals from small fluctuations in the baseline. This reduces the acquired raw data to two signal parameters: the zero-crossing time and the peak-to-peak amplitude of the filtered derivative. In the DST files, the signals are grouped by PPAC channel and by neutron pulse, making it possible to search for time coincidences in close detectors.

The internal clocks of the FADC digitizers, which have a nominal accuracy of 2 ppm, were calibrated with a pulse generator because of the high time precision required by the coincidence method. Differences of a few nanoseconds were measured among the FADC modules, being corrected by software as the DST files were written [10].

The reference time for the conversion from TOF to neutron energy was derived from the signals produced by the so-called γ-flash, that consists in γ rays and ultrarelativistic light particles generated when a proton pulse hits the lead target. By averaging these clearly identifiable signals from all PPAC anodes, a common start of the neutron burst could be obtained with a time spread of 1 ns. The width of the γ-flash limits the maximum neutron energy in our experiment to 1 GeV.

Once obtained the absolute neutron TOF, the effective flight path was determined by fitting some of the measured ^{235}U(n, f) resonances below 300 keV to their evaluated resonance energies. The calculated flight path at the ^{235}U target position, excluding the moderation length inside the lead target, was 183.072 m. The flight path for the other targets is obtained by shifting it according to the geometrical distance to ^{235}U position. An additional term depending on the neutron energy was included in the energy calibration to account for the moderation process. The accuracy of this method is of the order of the n_TOF energy resolution [14], better than 10^{-3} in the full resonance region, assuming that ^{235}U resonances are known with better accuracy. The accuracy of this energy calibration for the other targets in the setup has been checked with the first resonances of the ^{235}U contaminant present in the ^{234}U samples.

B. Fission event building

With our detection setup, fission events can be discriminated from background by demanding the coincidence detection in the two PPACs next to the corresponding target. The two fission fragments emitted reach the adjacent detectors and produce signals within a narrow coincidence window of 10 ns. The window is not centered at null time difference, because the setup symmetry is broken by the presence of the target backing, which slows down one of the fragments. In addition to the signal time, the anode amplitudes also allow us to discard multifragmentation events at high energies and random α-particle coincidences. This is a very powerful method for eliminating the background produced by α particles owing to sample radioactivity or by spallation reactions.

Occasionally, a proton pulse misses the lead target, producing a trigger signal but no neutrons. In such cases, we obtain blank triggers in which only background events are registered. The study of these triggers has shown that the background induced by neutrons produced in previous pulses and backscattered by the walls was negligible.

IV. CROSS-SECTION CALCULATION

We consider the energy-dependent counting rate to be the total number of fission events induced in a target by neutrons of a given energy during the full measuring time. It can be defined by the expression

$$C(E) = \Phi(E) N_{\text{at}} \sigma(E) \epsilon(E) + Bk(E), \qquad (1)$$

where $\sigma(E)$ is the fission cross section of the isotope, $\Phi(E)$ is the neutron fluence (n/cm^2) for the full measuring period, N_{at} is the total number of atoms in the target, $\epsilon(E)$ is the detection efficiency, and $Bk(E)$ stands for the counting rate from sample contaminants, which is subtracted as mentioned before.

Assuming that all samples are hit by the same neutron fluence and with the same beam spot size, the fluence could be determined by the counting rate of the ^{235}U reference sample,

$$\Phi'(E) = \Phi(E)\epsilon_{U5}(E) = \frac{C_{U5}(E)}{N_{U5}\sigma_{U5}^{\text{ENDF}}(E)}. \qquad (2)$$

In the resonance region, where the flux is almost flat in a logarithmic scale, we used a fit to eliminate the fluctuations owing to local differences between our ^{235}U data and the Evaluated Nuclear Data Files (ENDF) evaluation in the valleys between resonances and at the limits of the resolved resonance region. The ENDF/B-VII.0 evaluation of the ^{235}U cross section has been used for obtaining the flux, in addition to Japanese Evaluated Nuclear Data Library-High Energy File (JENDL-HE) above 30 MeV. Therefore, the cross section is obtained as

$$\sigma(E) = \frac{C(E)}{\Phi'(E) N_{\text{at}}} \frac{\epsilon_{U5}(E)}{\epsilon(E)}. \qquad (3)$$

For obtaining the cross sections in the continuum region, we have assumed that the fluence ratio between two targets cancels out, so that no direct flux is included here. Therefore, the cross-section ratios between the isotopes studied (a) and

reference samples (b) are obtained as

$$\frac{\sigma_a(E)}{\sigma_b(E)} = \frac{C_a(E)}{C_b(E)} \frac{N_b \epsilon_b(E)}{N_a \epsilon_a(E)}. \qquad (4)$$

As explained in Sec. II B, the target masses have been accurately measured and the ratio of the number of atoms is well-known. The remaining term, the detection-efficiency ratio, is explained in the following subsection.

A. Detection efficiency

The determination of the detection efficiency is a primary issue for each cross-section measurement. In our case, we take advantage of the simultaneous detection of both fission fragments to indisputably discriminate the fission events. However, the angular acceptance is reduced because the fragments must pass through absorbing layers to reach the sensitive part of the detectors: the larger the fragment emission angle, the thicker are the traversed layers. Therefore, according to simulations, the largest angle accepted is about $60°$ and the detection efficiency falls until 50% in the case of an isotropic angular distribution of the fission fragments. Nevertheless, according to Eqs. (3) and (4), it is not an accurate detection efficiency for each sample that is required for obtaining the cross sections, but the ratio between the efficiencies of the investigated and the reference sample. Because the geometry and the materials are virtually identical for all targets, the detection efficiency is expected to be almost equal for all of them. A number of small deviations were considered in the following way:

$$\frac{\epsilon_a(E)}{\epsilon_b(E)} = 1 + \delta_{\text{thick}} + \delta_{\text{inh}} + \delta_{\text{thresh}} + \delta W(E) + \delta_{\text{chem}}. \qquad (5)$$

These deviations are caused by the remaining differences concerning the thickness of the backing and of the detectors (δ_{thick}), the mass distribution of the samples (δ_{inh}), or the performance of the various detectors resulting in different detection thresholds (δ_{thresh}). Furthermore, the characteristics of the fission fragments, in particular the angular distribution, differ with the isotope and with the neutron energy [$\delta W(E)$]. This contribution will be extensively explained in the next subsection.

An additional difference between the neptunium and the uranium samples has been discovered by means of an accurate RBS analysis [11]. The oxygen and hydrogen contents per actinide atom in the uranium samples are larger than in the neptunium ones. After studying the effect of the target composition with the help of simulation codes [15], we have estimated that the efficiency for neptunium targets is, on average, about $2(\pm 1)\%$ larger than for uranium targets. This correction for the chemical composition is considered in Eq. (5) by the additional term δ_{chem}.

The effects caused by the chemical composition and the angular distribution cancel out when comparing counting rates from samples of the same isotope so that these ratios provide information about the three other contributions in Eq. (5). Figure 2 shows that the counting-rate ratios of each ^{237}Np sample with respect to the average value (solid lines) and the ratio between the two ^{234}U samples (dotted line)
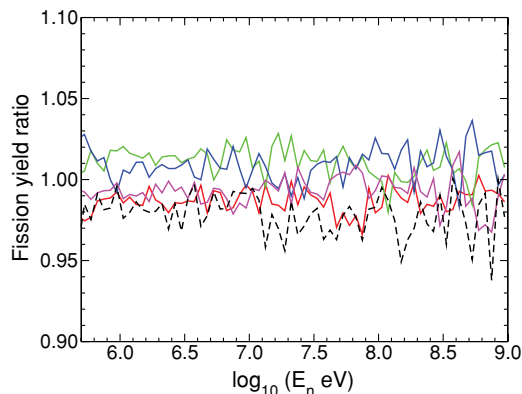
FIG. 2. (Color online) Fission yield ratios between different samples of the same isotope. The ratio between the two ^{234}U samples is shown by the dotted line, while the ratios between the neptunium samples and their average are indicated by solid lines. The fission yields are renormalized by the amount of mass in each target.

are practically constant. Therefore, we have assumed these deviations to be energy-independent. All the ratios remain within a 3% difference, including the neptunium sample with a different composition. The simulations performed show that the contribution of the two first terms is small, around 1.5% for the variations in the setup thicknesses and even less for the inhomogeneities in the samples, so that the main contribution is coming for the detection thresholds for each PPAC. These effects could not been corrected but they are taken into accout in the systematic uncertainty of the detection efficiency, shown in Tables II and III.

B. Anisotropy correction

The angular distribution of the fission fragments depends on the fissioning nuclei and the incident neutron energy. At low neutron energies, there is not a preferred direction for the fragments emitted, so the angular distribution is isotropic. However, for fast neutrons the emission becomes anisotropic, which affects the detection efficiency of the setup. The anisotropy behavior is rather smooth with the energy, except at the threshold energies of the different fission modes, where the anisotropy changes drastically.

TABLE II. Systematic uncertainties for ^{234}U obtained for this work data. Total uncertainty is provided for three different energy regions defined in the table.

Contribution	Uncertainties (%)
Sample mass	1.2
Thickness and threshold effects	3.6
Anisotropy	
(a) $E < 1$ MeV	1.2
(b) 1 MeV $> E > 6$ MeV	0.6
(c) $E > 6$ MeV	1
Total	(a) 4, (b) 3.8, (c) 3.9

TABLE III. Systematic uncertainties for ^{237}Np obtained for this work data. Total uncertainty is provided for two different energy regions defined in the table.

Contribution	Uncertainties (%)
Sample mass	1.1
Thickness and threshold effects	3.3
Oxygen content	1.0
Anisotropy	
(a) $E < 6$ MeV	0.5
(b) $E > 6$ MeV	1.0
Total	(a) 3.6, (b) 3.8

Because of the limited angular range of our detection setup, we can only obtain an extrapolated anisotropy value from our experimental data. Although the results reproduce qualitatively well the anisotropy behavior, the results are not accurate enough [10] to correct properly the angular distribution effect in the efficiency. Therefore, we have used the information on ^{235}U, ^{234}U, and ^{237}Np angular distributions from the Experimental Nuclear Reaction Data (EXFOR) database [16] to correct it. To consider the energy dependence of the anisotropy, a simple function fitting the EXFOR experimental data has been obtained for each sample as it is shown in Fig. 3. Above 20 MeV, there is no data available in EXFOR for these samples. Therefore, the anisotropy function in this region is constrained to follow the decreasing trend that is observed for ^{238}U and ^{232}Th experimental results [34].

Assuming that the fission fragment angular distribution can be approximately reproduced by $dW(\theta)/d\Omega \propto 1 + A \cos^2 \theta$, where θ is the emission angle with respect to the beam axis and the anisotropy factor in the center-of-mass frame A is defined as $W(0°)/W(90°) - 1$, we have used the expression

$$\frac{\int_{0.5}^{1} W(\theta) \, d(\cos \theta)}{\int_{0}^{1} W(\theta) \, d(\cos \theta)} \quad (6)$$

to estimate the reduction in the setup detection efficiency for each sample. The lower limit of the numerator integral corresponds to the cosine of the largest angle accepted by the detector. For large anisotropy values, the detection efficiency is higher than for isotropic emission. However, the variations in the efficiency ratio between the studied target and the reference one remain small. The calculated values for the efficiency ratio between ^{235}U and ^{234}U are shown in Fig. 4. Even when ^{234}U presents strong anisotropies, the difference in the target efficiency is not larger than 8%.

C. Systematic uncertainties

To provide an approximative estimation of the accuracy of the present results, we discuss in this section the main sources of systematic uncertainty. The largest contribution comes from the uncertainties in the detection efficiency related to the material thicknesses and inhomogeneities and, especially, the detector thresholds, which may amount to up to 3% for a single target, as previously shown. The difference in the oxygen content between uranium and neptunium targets
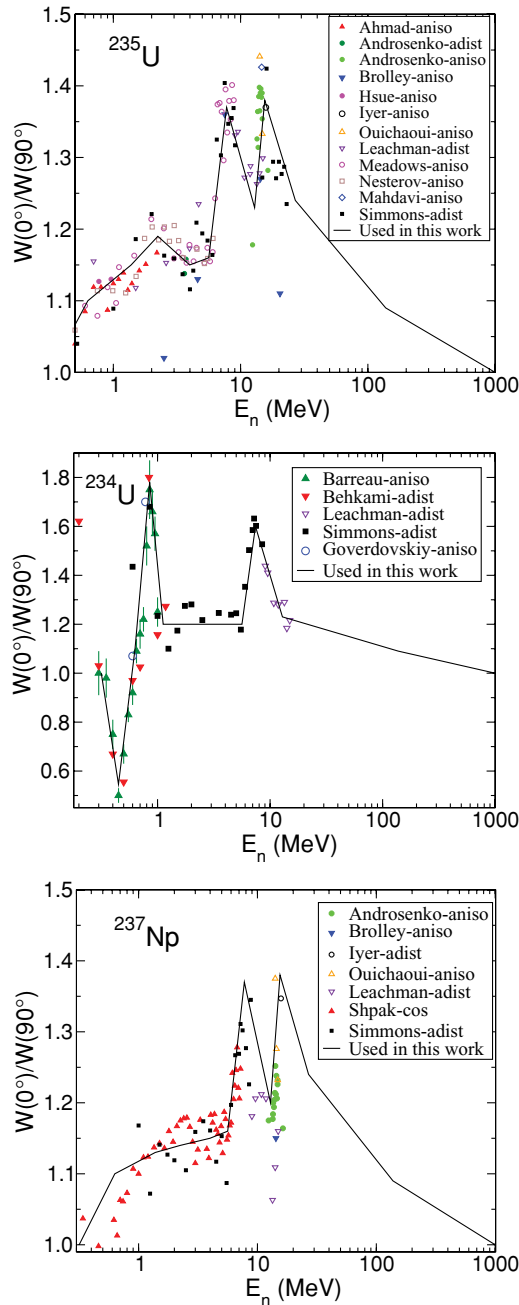
FIG. 4. Calculated energy-dependent efficiency ratio obtained for ^{235}U and ^{234}U targets. Larger deviations from the unity correspond to neutron energies near the ^{234}U fission threshold, where this isotope presents the largest anisotropy.

The systematic uncertainties in the sample mass determination were already provided in Table I, which result in contributions of 1.2% and 1.1% in the overall uncertainties of ^{234}U and ^{237}Np, respectively.

The total systematic uncertainty, shown in Tables II and III, remains below 4% in the fast-neutron region for both isotopes.

V. RESULTS AND DISCUSSION

The results obtained for the ^{234}U and ^{237}Np fission cross sections have been divided in two neutron-energy regions corresponding to the procedures used in the data analysis. This division matches approximately the resonance region and the continuum part where the cross sections exhibit a smooth trend with neutron energy. For both regions, we discuss our results compared to the evaluations in the nuclear databases ENDF [35,36], JENDL [37], and Joint Evaluated Fission and Fusion File (JEFF) [38], data obtained at 300 K, and experimental data from the EXFOR database.

A. Resonance region

Both isotopes, ^{234}U and ^{237}Np, are characterized by a small subthreshold cross section. However, significant resonances can be observed for these isotopes, which increase the fission probability at certain discrete energies.

In the case of ^{234}U, experimental data in the resonance region are scarce. Apart from the results of James *et al.* [39], a recent experiment at Geel [40] has been reported, but only in a reduced-energy region. The high resolution achieved at the n_TOF facility allowed us to resolve the subthreshold fission resonances with unprecedented accuracy. This is illustrated in Fig. 5 by comparison with the data of Refs. [39,40] and with evaluated data [35–37]. In general, there is fair agreement with the ENDF/B-VII evaluation except that resonance multiplets could now be resolved by the present data and a slight displacement of the resonance position is observed with respect to evaluated resonances.

For ^{237}Np a few high-resolution measurements have been reported so far [41–43]. The comparison of our results in Fig. 6 shows relatively good agreement with those of Ref. [42]

FIG. 3. (Color online) Experimental anisotropies obtained from the EXFOR database for the fission fragment angular distribution in neutron-induced fission of ^{235}U (top) [17–29], ^{234}U (middle) [25,29–32], and ^{237}Np (bottom) [19,21,23–25,29,33]. The solid lines represent the estimated anisotropy used in this work.

implies an extra contribution for ^{237}Np uncertainty that is about 1%.

The anisotropy correction partially cancels out and, therefore, the uncertainty is almost negligible in the regions where the anisotropy is small and similar for the studied and the reference targets, while the uncertainty in the correction remains below 2% in the regions with the largest anisotropy differences or where the angular distribution is roughly known.
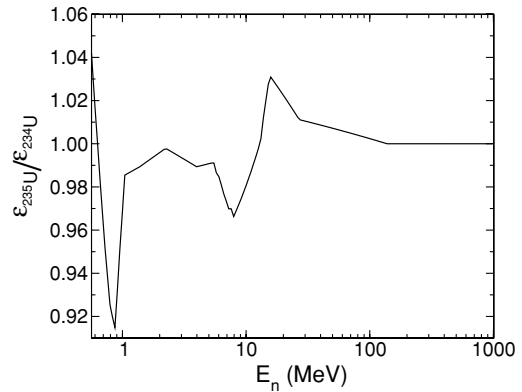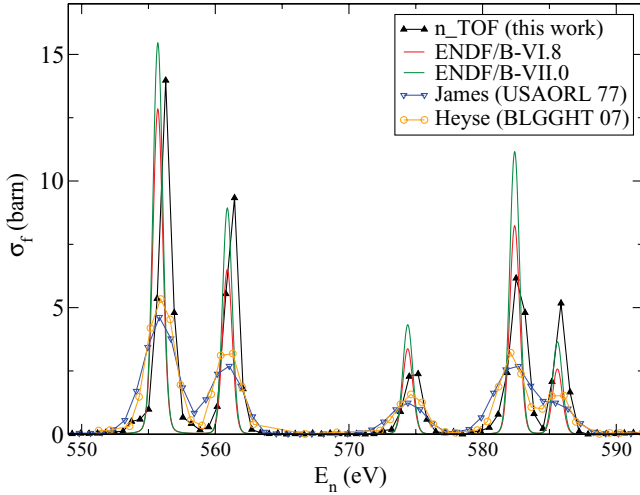
FIG. 5. (Color online) ^{234}U fission resonances around 500 eV. The present n_TOF data are shown in comparison with the ENDF/B-VI.8, ENDF/B-VII.0, and JEFF-3.1 evaluations. The data of James *et al.* [39] and Heyse *et al.* [40] are also included.

FIG. 6. (Color online) ^{237}Np fission resonances around 40 eV. n_TOF data are shown in comparison with the ENDF/B-VI.8, ENDF/B-VII.0, and JENDL-3.3 evaluations. We have also included data from Furman *et al.* [41], Auchampaugh *et al.* [42], and Plattard [43].

and the ENDF/B-VII and JENDL-3.3 evaluations, whereas the resonances are largely underestimated in ENDF/B-VI.

In Tables IV and V the averaged cross section in wider energy intervals is compared with the evaluations and the previous data. In the resolved resonance region, our values for ^{234}U are about 27% above the results obtained by James *et al.* [39]. Beyond 1.5 keV, the differences are greater up to
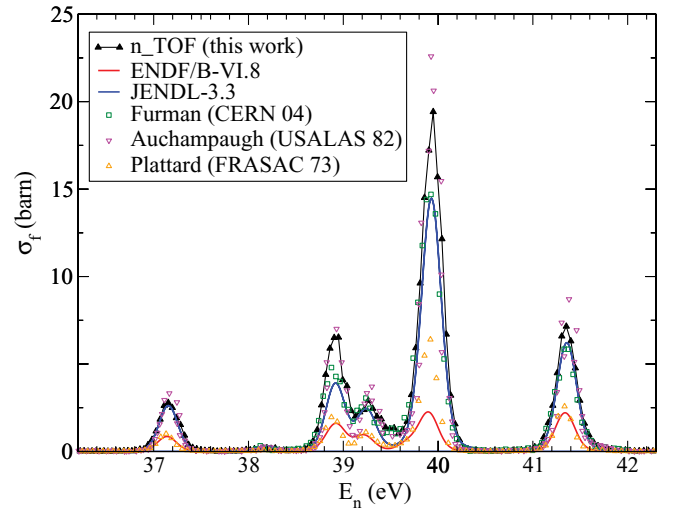
the fission threshold. Compared to evaluations, our data are closer to those of JENDL-3.3 than to the ENDF evaluations up to 1 keV.

In the case of ^{237}Np, our integrated data are approximately 10% higher than those of ENDF/B-VII.0 or JENDL-3.3 for the

TABLE IV. Energy-averaged cross sections for ^{234}U (in units of mbarn), with their statistical and systematic uncertainties, compared to evaluations and to the data of Ref. [39]. The ratios to the present results are given in parentheses.

E (eV)[a]	n_TOF	ENDF/B-VI.8	ENDF/B-VII.0	JENDL-3.3	James [39]
1–100	$49.0 \pm 0.3 \pm 2$	24.2(2.02)	30.4(1.61)	36.6(1.34)	38.7(1.27)
100–200	$120.0 \pm 1.6 \pm 4$	69.8(1.72)	89.1(1.34)	98.1(1.22)	93.8(1.28)
200–300	$39.3 \pm 1.2 \pm 1.6$	22.6(1.74)	30.2(1.30)	37.8(1.4)	33.3(1.18)
300–400	$77 \pm 2 \pm 2$	42.4(1.82)	56.3(1.37)	59.2(1.30)	61.0(1.26)
400–500	$299 \pm 5 \pm 12$	180.1(1.66)	228.6(1.31)	248.6(1.20)	234.0(1.28)
1–500	$117 \pm 0.5 \pm 4$	67.9(1.72)	87.0(1.34)	96.2(1.22)	92.3(1.27)
500–600	$806 \pm 9 \pm 28$	466.2(1.73)	609.4(1.32)	629.9(1.28)	621.6(1.30)
600–700	$228 \pm 5 \pm 8$	125.4(1.76)	171.2(1.29)	187.9(1.18)	185.4(1.23)
700–800	$87 \pm 3 \pm 3$	44.5(1.96)	59.6(1.46)	62.4(1.39)	71.9(1.21)
800–900	$59 \pm 3 \pm 2$	35.9(1.64)	45.7(1.29)	50.4(1.18)	50.2(1.18)
900–1000	$15.7 \pm 1.4 \pm 0.5$	9.6(1.64)	10.9(1.44)	11.7(1.34)	15.8(0.99)
0.500–1. (keV)	$239 \pm 2 \pm 8$	136.4(1.75)	179.0(1.34)	188.6(1.27)	188.6(1.27)
1–1.5	$20.5 \pm 0.8 \pm 0.7$	10.5(1.95)	13.2(1.55)	12.8(1.60)	16.4(1.25)
1.5–2	$7.0 \pm 0.5 \pm 0.2$	8.3(0.84)	6.4(1.09)	11.0(0.64)	4.4(1.59)
2–5	$12.0 \pm 0.4 \pm 0.4$	8.3(1.44)	6.5(1.84)	10.8(1.13)	9.9(1.21)
5–10	$23.9 \pm 0.7 \pm 0.9$	15.5(1.54)	12.2(1.96)	10.6(2.25)	15.3(1.56)
10–20	$21.0 \pm 0.7 \pm 0.8$	15.0(1.40)	11.7(1.79)	10.4(2.02)	15.0(1.40)
20–100	$21.9 \pm 0.4 \pm 0.9$	19.6(1.12)	14.7(1.49)	20.5(1.07)	15.7(1.39)
100–200	$43.1 \pm 0.7 \pm 1.7$	62.0(0.70)	44.0(0.98)	47.8(0.90)	42.3(1.02)
200–400	$124.2 \pm 1.1 \pm 5$	152.9(0.81)	120.9(1.03)	126.1(0.98)	144.9(0.86)
400–600	$538 \pm 2 \pm 21$	583(0.92)	541(0.99)	519(1.04)	608(0.88)
600–1000	$1062 \pm 2 \pm 42$	1164(0.91)	1109(0.96)	1134(0.94)	1069(0.99)

[a]Above 1500 eV the units change to keV.

TABLE V. Energy-averaged cross sections for ^{237}Np (in units of mbarn), with their statistical and systematic uncertainties, compared to evaluations. The ratios to the present results are given in parentheses.

E (eV)[a]	n_TOF	ENDF/B-VI.8	ENDF/B-VII.0	JENDL-3.3
1–100	$147.6 \pm 0.7 \pm 6$	36.3(4.07)	123.5(1.20)	123.4(1.20)
100–200	$67.6 \pm 0.9 \pm 2$	15.0(4.51)	63.7(1.06)	63.7(1.06)
200–300	$144 \pm 2 \pm 5$	50.9(2.83)	143.3(1.00)	143.0(1.01)
300–400	$60.4 \pm 1.5 \pm 2$	18.5(3.26)	58.0(1.04)	58.1(1.04)
400–500	$54.1 \pm 1.4 \pm 1.9$	17.9(3.01)	44.6(1.21)	44.6(1.21)
1–500	$94.7 \pm 0.4 \pm 4$	27.7(3.42)	86.6(1.09)	86.5(1.09)
500–600	$27.6 \pm 1.2 \pm 1.0$	7.2(3.83)	48.6(0.57)	48.8(0.56)
600–700	$36.4 \pm 1.5 \pm 1.3$	12.7(2.87)	47.4(0.77)	47.3(0.77)
700–800	$26.0 \pm 1.3 \pm 1.0$	10.4(2.50)	48.4(0.54)	48.3(0.54)
800–900	$82.3 \pm 2.5 \pm 3$	26.2(3.14)	49.6(1.66)	49.4(1.66)
900–1000	$3.6 \pm 0.5 \pm 0.1$	5.8(0.62)	51.0(0.07)	50.9(0.07)
0.5–1(keV)	$35.2 \pm 0.7 \pm 1.3$	12.5(2.82)	49.0(0.72)	48.9(0.72)
1–1.5	$50.4 \pm 1.0 \pm 1.8$	14.3(3.52)	48.3(1.04)	48.5(1.03)
1.5–2	$30.7 \pm 1.0 \pm 1.1$	7.6(4.04)	40.1(0.76)	40.4(0.76)
2–5	$21.6 \pm 0.5 \pm 1.0$	9.2(2.34)	29.6(0.73)	29.8(0.72)
5–10	$18.5 \pm 0.5 \pm 0.7$	8.6(2.15)	22.1(0.84)	22.3(0.83)
10–20	$15.2 \pm 0.4 \pm 0.6$	9.2(1.65)	17.5(0.87)	18.1(0.84)
20–100	$16.8 \pm 0.3 \pm 0.6$	12.0(1.40)	16.0(1.05)	16.7(1.01)
100–200	$26.3 \pm 0.4 \pm 1.0$	22.0(1.20)	25.5(1.03)	24.6(1.07)
200–400	$73.1 \pm 0.6 \pm 3$	74.9(0.98)	80.1(0.91)	76.5(0.96)
400–600	$451.4 \pm 1.4 \pm 16$	393.8(1.14)	422.0(1.05)	409.5(0.97)
600–1000	$1200.7 \pm 1.5 \pm 43$	1120.7(1.08)	1168.7(1.03)	1171.6(1.03)

[a]Note: Above 1000 eV the units change to keV.

resolved resonance region; while for the unresolved resonance region our data are clearly lower than both evaluations up to 20 keV. The ENDF/B-VI.8 evaluation strongly underestimates the cross section below 200 keV.

B. Above the fission threshold

The present results are the only data extending to 1 GeV. Because the standard references become less reliable at these high energies, we also provide our cross section ratios with respect to ^{235}U for inclusion into the EXFOR database.

In Fig. 7 the ^{234}U cross section is compared to evaluations and to experimental data. Most data from the EXFOR database are ratios relative to ^{235}U. These have been converted to cross sections using the recommended IAEA standard cross section for ^{235}U [48]. To represent our data, we have chosen a variable number of bins per energy decade (200 bins/decade below 10 MeV, 100 bins/decade up to 100 MeV, and 50 bins/decade above 100 MeV). Therefore, the statistics are enough above the fission threshold to reach statistical uncertainties below 4% in the entire region. Although the binning does not allow us to distinguish fine details in the resonance-like structure around 300 keV pointed out by James *et al.* [39], it is still sufficient to confirm the existence of that structure.

Most previous measurements have been performed in the energy range between 0.5 and 10 MeV. In general, our data are in good agreement with those of Fursov *et al.* [49], Meadows [50], Behrens and Carlson [46], and White and Warner [47]. Some of them are shown in Fig. 7 to compare

with our results. Discrepancies are found when comparing our results with those of James *et al.* [39], and even more when compared with those of Lisowski *et al.* [44], which are systematically higher than all other measurements. The
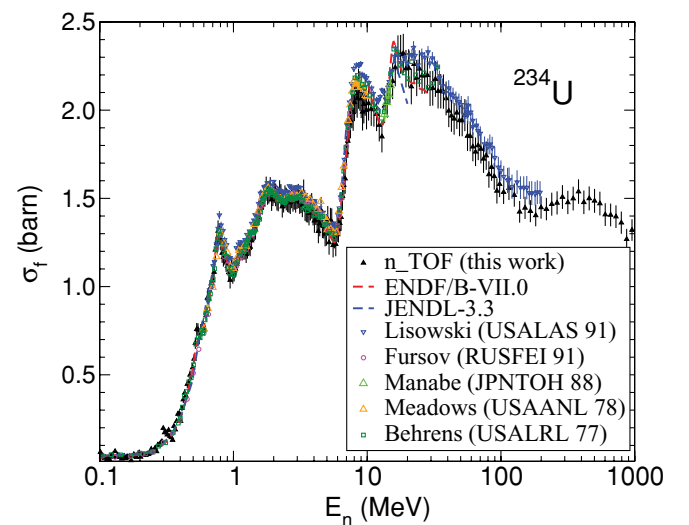

FIG. 7. (Color online) The fission cross section of ^{234}U from threshold to 1 GeV compared to the ENDF/B-VII.0 and the JENDL-3.3 evaluations and to selected experimental data [39,44–47]. The error bars of the present data correspond to the statistical and systematic uncertainties.
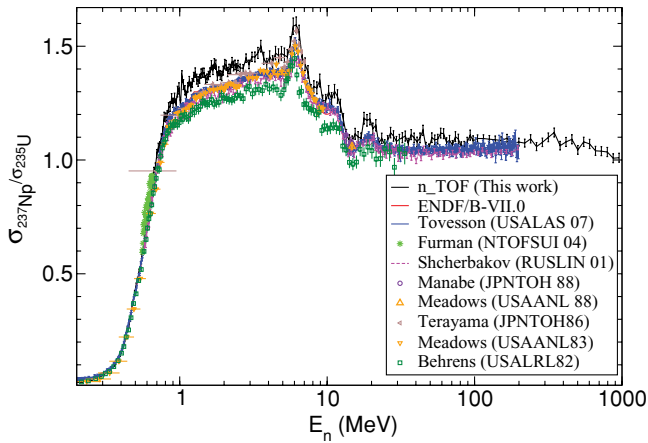
FIG. 8. (Color online) The fission cross section ratio of ^{237}Np relative to ^{235}U from threshold to 1 GeV compared to the ENDF/B-VII.0 evaluation and to selected experimental data [41,53,56,58,60,62]. The error bars of the present data correspond to the statistical uncertainties only.

FIG. 9. (Color online) The fission cross section of ^{237}Np from threshold to 1 GeV. n_TOF data compared to the ENDF/B-VII.0 and JEFF-3.1 evaluations and to selected experimental data [52,54,55,58,63]. The error bars of the present data correspond to the statistical and systematic uncertainties.

good agreement with the other data sets in the first chance region, where the ^{234}U anisotropy reaches its maximum value, supports our detection efficiency correction. Above 10 MeV data are rather scarce and only the measurement of Lisowski extends up to 400 MeV. The systematic shift of these data is also present in the high-energy region, where present results are in good agreement with Behrens and Carlson [46] and Manabe *et al.* [45].

Compared to the existing evaluations, our data are in good agreement with ENDF/B-VII.0 up to 15 MeV, except for small discrepancies in the region of the second and third fission chances. Larger differences are found with respect to the JENDL-3.3 evaluation.

For ^{237}Np the present fission cross-section data are compared to the ENDF/B-VII.0 and the JENDL-3.3 evaluations. The cross-section shape was found to agree with ENDF/B-VII.0, but our cross-section values are systematically higher by about 3% below and 6% above 1 MeV. Even larger differences of 8% are found above 6 MeV with respect to JENDL-3.3, significantly beyond the 3%–4% systematic uncertainty of the present data.

When compared to the large body of experimental results [51], our data are in agreement with most of the experiments performed with monoenergetic sources around 14 MeV as those from Manabe [45], Alknazov [52], Meadows [53], or Garlea [54]. They are also close to those of Jiacoletti *et al.* [55] (up to 5 MeV) and Terayama *et al.* [56] (above 4 MeV), but lower than those of Furman *et al.* around 600 keV [41] and those of Pankratov *et al.* [57] above the second-chance fission threshold and higher than what was reported by Shcherbakov *et al.* [58], Meadows [59], and Behrens *et al.* [60]. The results of Lisowski *et al.* [61] are normalized to those of Meadows [59] over the 1- to 10-MeV energy range. The recent results obtained from Tovesson and Hill [62] are also normalized to the ENDF/B-VI evaluation, which also follows the results of Meadows. They are included in Fig. 8 to compare the shape of the excitation function above 30 MeV.
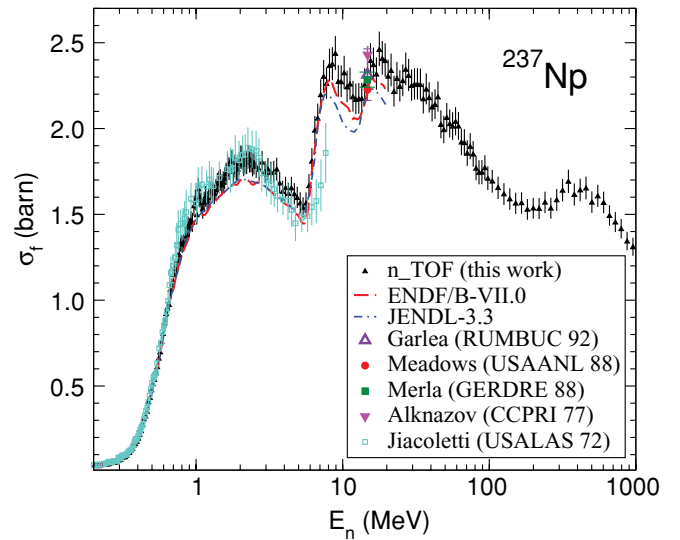
At energies from 20 to 100 MeV, our data follow the same decreasing trend as those of Shcherbakov *et al.* [32], similar to what was found for ^{234}U. Both isotopes present a constant cross section ratio relative to ^{235}U beyond 30 MeV.

It is worth mentioning that the present results are supported by the fact that we could reproduce in the same experiment the standard fission cross section of ^{238}U within the achieved uncertainty of $\pm3\%$ [11].

VI. SUMMARY AND CONCLUSIONS

The ^{234}U(n,f) and ^{237}Np(n,f) cross sections were studied for neutron energies from 1 eV to 1 GeV at the n_TOF facility. Fission fragments from very thin samples were detected in coincidence with PPACs. The cross sections were obtained relative to ^{235}U, using the ENDF/B-VII.0 evaluation as a reference. However, as the ^{235}U fission cross section is considered as a standard only up to 20 MeV, the ratios relative to ^{235}U are provided too. Unlike in some other experiments, the present results have not been normalized to previous data or evaluations.

In general, the results for ^{234}U(n,f) are in good agreement with previous data except for the differences in the resonance region, where there is a lack of recent experimental data. We think that our excellent energy resolution will lead to improvement in the resonance parameters, in particular, the resonance positions. Above the fission threshold, our results support current evaluations, extending the range of available data up to 1 GeV.

However, for ^{237}Np(n,f) our data exhibit significant discrepancies compared to recent evaluations, although the cross-section shape is quite similar. The measurement and data analysis have been checked in detail, the detection efficiency was carefully corrected and our results are supported by the

fact that the ^{238}U and the ^{234}U fission cross section could be well reproduced within the experimental uncertainties of 3%. Therefore, the present work may be useful for improving the existing evaluations.

[1] M. Salvatores, NEA/WPEC-26, NEA/OECD, Paris, 2008.

[2] A. Plompen and A. Mengoni, Summary Report of Consultants Meeting on Minor Actinide Nuclear Reaction Data (MANREAD), INDC(NDS)-0512, IAEA-NDS, Vienna, 2007.

[3] C. Stephan and P. Cennini, CERN-INTC-2003-021, CERN, Geneva, 2003.

[4] C. Stephan, CERN-INTC-2001-025, CERN, Geneva, 2001.

[5] C. Stephan, L. Ferrant, B. Berthier, S. David, L. Tassan-Got, C. Bacri, F. Rejmund, and C. Moreau (n_TOF Collaboration), J. Nucl. Sci. Tech. Suppl. **2**, 276 (2002).

[6] L. Tassan-Got, B. Berthier, I. Duran, L. Ferrant, S. Isaev, C. de la Naour, C. Paradela, C. Stephan, and D. Trubert (n_TOF Collaboration), in *Proceedings of the International Conference on Nuclear Data for Science and Technology, Santa Fe, 2004*, edited by R. Haight, M. Chadwick, T. Kawano, and P. Talou (American Institute of Physics, College Park, MD, 2005), p. 1529.

[7] C. Borcea *et al.*, Nucl. Instrum. Methods Phys. Res. A **513**, 524 (2003).

[8] (n_TOF Collaboration), Proposal for a neutron TOF facility, CERN/SPSS 99-08, SPSC/P310, CERN, Geneva, 1999.

[9] (n_TOF Collaboration), n_TOF Technical Report, CERN/INTC 2000-018, CERN SPSC/P310, CERN, Geneva, 2000.

[10] C. Paradela, Ph.D. work, Universidad de Santiago de Compostela, 2005, [http://fpsalmon.usc.es/PhDthesis/Tesis_carlos.pdf].

[11] L. Tassan-Got, L. Audouin, B. Berthier, I. Duran, S. Isaev, C. Paradela, and C. Stephan (unpublished).

[12] L. Ferrant, Ph.D. work, Université Paris-Sud, 2005.

[13] U. Abbondanno *et al.*, Nucl. Instrum. Methods Phys. Res. A **538**, 692 (2005).

[14] C. Coceva, M. Frisoni, M. Magnani, and A. Mengoni, Nucl. Instrum. Methods Phys. Res. A **489**, 346 (2002).

[15] J. Ziegler, J. Biersack, and U. Littmark, *The Stopping and Range of Ions in Solids* (Pergamon Press, New York, 1985).

[16] *Experimental Nuclear Reaction Data (EXFOR)* (National Nuclear Data Center, Brookhaven, NY, 2009) [http://www-nds.iaea.org/exfor/exfor.htm].

[17] S. Ahmad, M. Islam, A. Khan, M. Khaliquzzaman, M. Husain, and M. Rahman, Nucl. Sci. Eng. **71**, 208 (1979).

[18] K. Androsenko, G. Korolev, and D. Shpak, Yad. Konstanty **1985**, 24 (1985).

[19] K. Androsenko, G. Korolev, and D. Shpak, Yad. Konstanty **46**, 9 (1982).

[20] J. E. Brolley Jr., W. Dickinson, and R. L. Henkel, Phys. Rev. **99**, 159 (1955).

[21] J. E. Brolley Jr. and W. Dickinson, Phys. Rev. **94**, 640 (1954).

[22] S. Hsue, G. Knoll, and J. Meadows, Nucl. Sci. Eng. **66**, 24 (1978).

[23] R. Iyer and M. Sagu, in *Proceedings of Nuclear and Solid State Physics Symposium, Madurai 1970* (1970), Vol. 2, p. 57.

[24] S. Ouichaoui, S. Juhasz, M. Varnagy, and J. Csikai, Acta Phys. Acad. Sci. Hung. **64**, 209 (1988).

[25] R. B. Leachman and L. Blumberg, Phys. Rev. **137**, B814 (1965).

[26] J. Meadows and C. Budtz-Jorgensen, Argonne National Laboratory Report No. 64. ANL/NDM-64, January 1982.

[27] M. Mahdavi, G. Knoll, and J. Robertson, Trans. Am. Nucl. Soc. **44**, 532 (1983).

[28] V. Nesterov, G. Smirenkin, and D. Shpak, Yad. Fiz. **4**, 993 (1966).

[29] J. E. Simmons and R. Henkel, Phys. Rev. **120**, 198 (1960).

[30] G. Barreau, C. E. N. Bordeaux-Gradignan Report No. 7706, 1977.

[31] A. Behkami, J. Roberts, W. Loveland, and J. Huizenga, Phys. Rev. **171**, 1267 (1968).

[32] A. Goverdovskiy, A. Gordyushin, B. Kuzminov, V. Mitrofanov, and A. Sergachev, At. Energy **62**, 190 (1986) [Sov. At. Energy **62**, 238 (1987)].

[33] D. Shpak, B. Fursov, and G. Smirenkin, Yad. Fiz. **12**, 35 (1970) [Sov. J. Nucl. Phys. **44**, 179 (1986)].

[34] G. Tutin, I. Ryzhov, V. Eismont, A. Kireev, H. Conde, K. Elmgren, N. Olsson, and P.-U. Renberg, Nucl. Instrum. Methods Phys. Res. A **457**, 646 (2001).

[35] CSEWG Collaboration, 2001 [www.nndc.bnl.gov/endf].

[36] M. B. Chadwick *et al.*, Nucl. Data Sheets **107**, 2931 (2006).

[37] K. Shibata *et al.*, J. Nucl. Sci. Technol. **39**, 1125 (2002).

[38] The JEFF3.1 Nuclear Data Library, JEFF Report 21, NEA/OECD No. 6190, OECD/NEA Data Bank, Paris, France, 2006.

[39] G. James, J. Dabbs, J. Harvey, N. Hill, and R. Schindler, Phys. Rev. C **15**, 2083 (1977).

[40] J. Heyse, C. Wagemans, L. D. Smet, O. Serot, J. Wagemans, and J. V. Gils, Nucl. Sci. Eng. **156**, 211 (2007).

[41] W. Furman *et al.*, *Proceedings of Conference on Nuclear Data for Science and Technology, Santa Fe 2004* (American Institute of Physics, College Park, MD, 1984), p. 1039.

[42] G. F. Auchampaugh, M. S. Moore, J. D. Moses, R. O. Nelson, R. C. Extermann, C. E. Olsen, N. W. Hill, and J. A. Harvey, Phys. Rev. C **29**, 174 (1984).

[43] T. Plattard, Ph.D. thesis, Saclay, 1973.

[44] P. Lisowski, A. Gavron, W. Parker, S. Balestrini, A. Carlson, O. Wasson, and N. Hill, *Conference on Nuclear Data for Science Technology, Juelich* (American Institute of Physics, College Park, MD, 1991), p. 732.

[45] F. Manabe, K. Kanda, T. Iwasaki, H. Terayama, Y. Karino, M. Baba, and N. Hirakawa, Tohoku Univ. Tech. Rep. **52**, 97 (1988).

[46] J. Behrens and G. Carlson, Nucl. Sci. Eng. **63**, 250 (1977).

[47] P. White and G. Warner, J. Nucl. Energy **21**, 671 (1967).

[48] A. D. Carlson, *International Evaluation of Neutron Cross-section Standards* (International Atomic Energy Agency, New York, 2007).

[49] B. Fursov, E. Y. Baranov, M. P. Klemyshev, B. Samylin, G. Smirenkin, and Y. Turchin, At. Energ. **71**, 827 (1992).

[50] J. Meadows, Nucl. Sci. Eng. **65**, 171 (1978).

[51] *Computer Index of Nuclear Reaction Data (CINDA)* (OECD Nuclear Agency, Paris, 2007).

[52] I. Alknazov, S. Kovalenko, O. Kostochkin, L. Malkin, K. Petrzhak, A. Sokolov, A. Fomichev, and V. Shpakov, Conf. Neutron Phys. **3**, 115 (1977).

[53] J. W. Meadows, Ann. Nucl. Energy **15**, 421 (1988).

[54] I. Garlea, C. Miron-Garlea, H. Rosu, G. Fodor, and V. Raducu, Rev. Roum. Phys. **37**, 19 (1992).

[55] R. Jiacoletti, W. Brown, and H. Olson, Nucl. Sci. Eng. **48**, 412 (1972).

[56] H. Terayama, Y. Karino, F. Manabe, M. Yanagawa, K. Kanda, and N. Hirakawa, Tohoku Univ. Dep. Nucl. Eng. Rep. No. 47 (1986).

[57] V. Pankratov, N. Vlasov, and B. Rybakov, At. Energ. **9**, 399 (1960) [Sov. J. At. Energy **9**, 939 (1961)].

[58] O. Shcherbakov *et al.*, J. Nucl. Sci. Tech. Suppl. **2**, 230 (2002).

[59] J. W. Meadows, Nucl. Sci. Eng. **85**, 271 (1983).

[60] J. Behrens, J. Browne, and J. Walden, Nucl. Sci. Eng. **80**, 393 (1982).

[61] P. Lisowski, J. Ullmann, S. Balestrini, A. Carlson, O. Wasson, and N. Hill, *Conference on Nuclear Data For Science and Technology, Mito 1988*, edited by S. Igarasi (Japan Atomic Energy Research Institute, 1998), p. 97.

[62] F. Tovesson and T. Hill, Phys. Rev. C **75**, 034610 (2007).

[63] K. Merla, P. Hausch, C. Herbach, G. Musiol, G. Pausch, U. Todt, L. Drapchinskiy, V. Kalinin, and V. Shpakov, in *Proceedings of the International Conference on Nuclear Data for Science and Technology, Juelich, Germany, (1991)*, edited by R. Haight, M. Chadwick, T. Kawano, and P. Talou (American Institute of Physics, College Park, MD, 2005), p. 510.